ARTICLE

BIOTECHNOLOGY and BIOENGINEERING

Zonal Rate Model for Axial and Radial Flow Membrane Chromatography, Part II: Model-Based Scale-Up

Pranay Ghosh,[1] Min Lin,[2] Jens H. Vogel,[2] Derek Choy,[3] Charles Haynes,[3] Eric von Lieres[1]

[1]IBG-1: Biotechnology, Forschungszentrum Jülich, Wilhelm-Johnen-Straße 1 52425, Jülich, Germany; telephone: +49-2461-61-2168; fax: +49-2461-61-3870; e-mail: e.von.lieres@fz-juelich.de

[2]Isolation and Purification Department, Global Biologics Development, Bayer Healthcare, Berkeley, CA

[3]Michael Smith Laboratories, University of British Columbia, Vancouver, Canada Boehringer Ingelheim, Fremont, CA

ABSTRACT: Membrane chromatography (MC) systems are finding increasing use in downstream processing trains for therapeutic proteins due to the unique mass-transfer characteristics they provide. As a result, there is increased need for model-based methods to scale-up MC units using data collected on a scaled-down unit. Here, a strategy is presented for MC unit scale-up using the zonal rate model (ZRM). The ZRM partitions an MC unit into virtual flow zones to account for deviations from ideal plug-flow behavior. To permit scale-up, it is first configured for the specific device geometry and flow profiles within the scaled-down unit so as to achieve decoupling of flow and binding related non-idealities. The ZRM is then configured for the preparative-scale unit, which typically utilizes markedly different flow manifolds and membrane architecture. Breakthrough is first analyzed in both units under non-binding conditions using an inexpensive tracer to independently determine unit geometry related parameters of the ZRM. Binding related parameters are then determined from breakthrough data on the scaled-down MC capsule to minimize sample requirements. Model-based scale-up may then be performed to predict band broadening and breakthrough curves on the preparative-scale unit. Here, the approach is shown to be valid when the Pall XT140 and XT5 capsules serve as the preparative and scaled-down units, respectively. In this case, scale-up is facilitated by our finding that the distribution of linear velocities through the membrane in the XT140 capsule is independent of the feed flow rate and the type of protein transmitted. Introduction of this finding into the ZRM permits quantitative predictions of breakthrough over a range of industrially relevant operating conditions.

Biotechnol. Bioeng. 2014;111: 1587–1594.

KEYWORDS: membrane chromatography; scale-up; modeling

The present address of Pranay Ghosh is Hoffmann-La-Roche AG, Basel, Switzerland
The present address of Jens H. Vogel is Boehringer Ingelheim, Fremont, CA
Correspondence to: E. von Lieres

Contract grant sponsor: Cluster for Industrial Biotechnology (CLIB)
Contract grant sponsor: NSERC, the Natural Sciences and Engineering Research Council of Canada
Received 13 December 2013; Revision received 31 January 2014; Accepted 3 February 2014
Accepted manuscript online 19 February 2014;
Article first published online 13 May 2014 in Wiley Online Library (http://onlinelibrary.wiley.com/doi/10.1002/bit.25217/abstract).
DOI 10.1002/bit.25217

Introduction

Membrane chromatography (MC) is increasingly used in industry as an alternative purification platform to packed bed chromatography (Boi et al., 2007; Ghosh, 2001; Ghosh and Wong, 2006; Vogel et al., 2012). Due to larger pore sizes, slow pore diffusion processes are essentially eliminated, leading to higher mass-transfer rates, and reduced overall operational times. The rate of column loading in a MC system is mainly governed by protein convection and either the thermodynamics or the rates of protein–sorbent complex formation (Briefs and Kula, 1992; Charcosset, 2006; Suen and Etzel, 1994). However, it is known that column-loading profiles of MC systems can deviate from the desired plug-flow behavior and can be strongly asymmetrical in nature under certain operating conditions (Montesinos-Cisneros et al., 2007; Sarfert and Etzel, 1997; Yang and Etzel, 2003). Experimental breakthrough curves (BTCs) typically show a sharp initial breakthrough that is followed by a slow approach to saturation. Such non-ideal behavior has been subject to active research for many years.

In the past, the asymmetric band broadening has been attributed mainly to complex protein binding mechanisms. These mechanisms have been modeled by many groups using different hypotheses such as multi-site, spreading, random-sequential adsorption, and steric mass-action/hindrance isotherm or rate models (Boi et al., 2007; Briefs and Kula, 1992; Brooks and Cramer, 1992; Clark et al., 2007; Lundstrom, 1985; Suen and Etzel, 1992; Talbot et al., 2000). In previous publications, we have shown that the spreading model, which hypothesizes different binding orientations of protein, can accurately describe the adsorption of bovine serum albumin (BSA) and ovalbumin on polyethersulfone membrane (PES) membranes coated with a cross-linked polymer containing pendant Q groups (Francis et al., 2011, 2012; Ghosh et al., 2013a). As well, Sarti and co-workers have shown that the bi-Langmuir model can accurately reproduce BTC data of BSA on cellulose acetate surfaces (Dimartino et al., 2011).

In addition to non-ideal binding, it has been observed that hold-up volumes within MC capsules, which are often as large as the membrane volume itself, can contribute significantly to system dispersion. This particularly holds for low-volume lab-scale MC capsules with an axial flow configuration, where solute molecules break through the central membrane area much earlier than through outer radial regions, and the resulting elution profiles can appear highly dispersed (Ghosh and Wong, 2006). However, the magnitude of these hold-up-volume related non-idealities does not necessarily scale due to the often vastly different manifold and membrane geometries used in scaled-down and preparative-scale units. Indeed, we have previously reported pronounced differences in band broadening within lab-scale (Pall Mustang XT5 with 5 mL membrane volume), and preparative-scale (Pall Mustang XT140 with 140 mL membrane volume) MC capsules containing the same membrane and operated at the same mean linear velocities (Fig. 1) (Ghosh et al., 2013a). Variations in the manifold design of the two MC capsules were identified as the major cause of the observed non-linear scaling between these capsules. Hence, any mathematical approach for model-based analysis and scale-up of MC units must carefully decouple the impacts of different non-idealities, including those caused by protein binding and by manifold and membrane architecture, on breakthrough performance.

We have previously developed a semi-empirical modeling approach, the zonal rate model (ZRM) (Francis et al., 2011, 2012; Ghosh et al., 2013a; von Lieres et al., 2009), for decoupling the contributions to band broadening of non-ideal hydrodynamics and binding in MC capsules. In the first paper of this series, the ZRM was thereby applied to systematically analyze lab-scale Mustang XT5 capsules. A more limited study of the preparative-scale XT140 capsule was also reported. Variations in protein residence times within the inlet and elution manifolds of both units were recorded, with the nature of the non-idealities unit-specific due the different flow geometries employed. In addition, variations in the linear velocity through the membrane stack

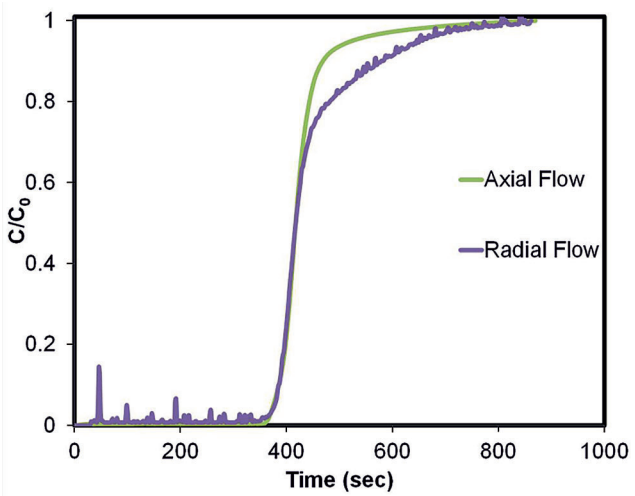

Figure 1. Breakthrough curves obtained under binding conditions for lab-scale axial-flow and production-scale radial-flow MC capsules with 1 mg/mL BSA at a flow rate of 12 MV/min.

were recorded in the preparative-scale capsule due in part to the radial-flow pleated membrane geometry employed. Those latter variations were shown to impact BTCs under binding conditions, while making relatively little contribution to band broadening under non-binding conditions. Here, we show that the relative distribution of linear velocities is independent of both the volumetric flow rate and the characteristics of the transmitted protein. When this knowledge is introduced into the ZRM, quantitative prediction of protein BTCs within production-scale MC capsules is then demonstrated over a range of industrially relevant operating conditions. Predictions are based on binding parameters determined in the scaled-down unit yielding a new cost-effective model-based method for scale-up and simulation of production-scale MC units.

Theory

Traditionally, MC has been modeled assuming flow homogeneity (linear velocities and mean residence times) within hold-up volumes upstream and downstream of the membrane stack and also over membrane cross sections. The hold-up volumes are therefore usually modeled by a linear combination of one or two continuously stirred tank regions (CSTR) and a plug flow region (PFR). The Roper and Lightfoot model (RLM) captures system dispersion by differently sized CSTRs on each side of the membrane (Roper and Lightfoot, 1995). The RLM, although adequate for modeling some cases, is based on a rather simplified representation of the true physical geometry of these systems.

Zonal Rate Model

The ZRM is designed to quantitatively capture the impact of inhomogeneous flow in MC capsules. To predict BTCs under

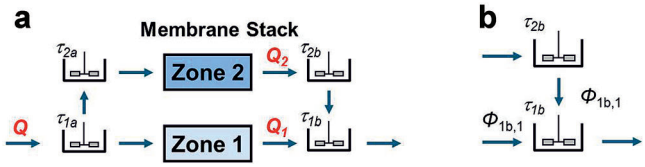

Figure 2. **a**: Virtual partitioning of hold-up volumes and membrane for the lab-scale axial-flow capsule, and (**b**) flow fractions of the collecting tank downstream of the membrane.

binding conditions, it requires a binding model, and the Langmuir, steric mass action (SMA), and spreading models have previously been integrated into the ZRM. A detailed mathematical description of the ZRM can be found in previous publications (Francis et al., 2011, 2012; von Lieres et al., 2009). Here, we therefore only describe configurations of the ZRM for the lab-scale Pall Mustang XT5 capsule (axial flow, see Fig. 2a) and the production-scale Pall Mustang XT140 capsule (radial flow, see Fig. 3a). Detailed information on the internal geometry of both capsules has been reported in a previous publication (Ghosh et al., 2013a). For the lab-scale capsule, the ZRM conceptually partitions the hold-up volumes before and after the membrane into two virtual flow zones. The membrane stack is also partitioned into two virtual zones having the same physical properties but subject to different boundary conditions. The inter-connected virtual zones for the hold-up volumes are modeled as a CSTR network, while each of those within the membrane stack are described by the one-dimensional mass continuity equation of chromatography:

$$\frac{\partial c}{\partial t} = -v\frac{\partial c}{\partial z} + D_a\frac{\partial^2 c}{\partial z^2} - \frac{1-\varepsilon}{\varepsilon}\frac{\partial q}{\partial t} \tag{1}$$

Here c and q are the solute concentrations in the mobile and stationary phases, respectively, z is the axial coordinate, v is the interstitial fluid velocity, D_a is the axial dispersion coefficient, and ε is the membrane porosity. We have previously shown with the help of infrared spectroscopy that the bulk porosity is rather homogeneous across the entire cross-section and thickness of the membranes used in this study (Johannes Kiefer et al., 2014). As is typical for chromatography modeling, solution of Equation (1) requires coupling to an appropriate protein-binding rate or isotherm model (see Binding Kinetics). Finally, the ZRM adds a plug flow region (PFR) in series with the CSTR network to model any time lag that is not associated with system dispersion (the time lag $t_{lag} = V_{PFR}/Q$ is the ratio of the PFR volume V_{PFR} to the volumetric feed flow rate Q):

$$c_{out}(t) = c_{in}(t - t_{lag}) \tag{2}$$

Due to its partitioning of the system into virtual zones, the ZRM requires a set of flow fractions, Φ_k, which define the fraction of the total volumetric flow passing through each of the membrane zones (Fig. 2b). Solute dispersion in the virtual zones upstream and downstream of the membrane stack is described by a conventional CSTR equation ($\tau = V_{CSTR}/Q$ is the average residence time, and j is the number of inflows of the respective CSTR):

$$\frac{\partial c_{out}}{\partial t} = \sum_{j=1}^{m}\frac{c_{in,j} - c_{out}}{\tau_j} \tag{3}$$

For the production-scale capsule, one virtual zone was found to be sufficient for capturing the flow behavior in the hold-up volumes before and behind the membrane region (Fig. 3a) (Ghosh et al., 2013a). However, the membrane zone had to be divided into several sectors with different linear velocities (Fig. 3a, only three sectors are shown for clarity of the sketch). These sectors represent specific regions of the pleated membrane, each characterized by unique structural attributes such as bed height and frontal area. Protein transport in each sector of the membrane is computed by solution of Equation (1) with the boundary conditions remaining constant across sectors and the distribution of linear velocities varying as a Gaussian-type function reported in Figure 3b.

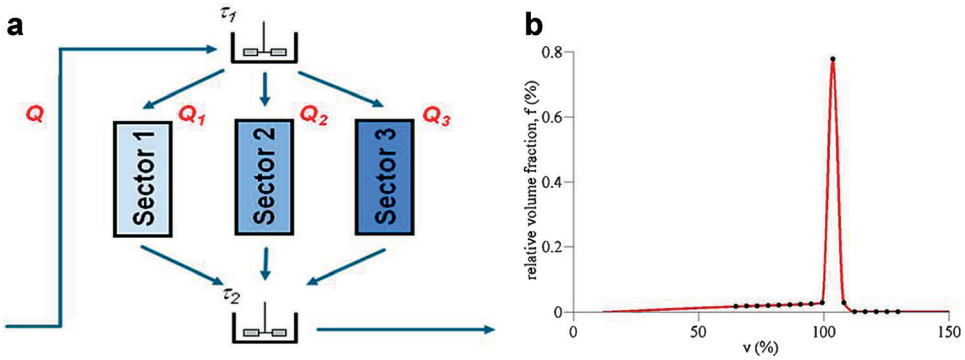

Figure 3. **a**: Virtual partitioning of hold-up volumes and membrane for the production-scale radial-flow capsule, where the membrane zone is split into sectors with varying linear velocities, and (**b**) distribution of the relative volumetric flow, *f*, over the relative linear velocity, *v*, in the respective sector.

Binding Kinetics

The kinetic form of the spreading model has been previously shown to accurately correlate BTC data for BSA eluting from a XT5 capsule (Francis et al., 2011, 2012; Ghosh et al., 2013a). That model assumes two different bound states, yielding rate equations of the form (Clark et al., 2007; Yang and Etzel, 2003):

$$\frac{\partial q}{\partial t} = \frac{\partial q_1}{\partial t} + \frac{\partial q_2}{\partial t} \quad (4)$$

$$\frac{\partial q_1}{\partial t} = (k_{a,1}c - k_{12}q_1)(q_m - q_1 - \beta q_2) - k_{d,1}q_1 + k_{21}q_2 \quad (5)$$

$$\frac{\partial q_2}{\partial t} = (k_{a,2}c + k_{12}q_1)(q_m - q_1 - \beta q_2) - (k_{21} - k_{d,2})q_2 \quad (6)$$

Here q_1 and q_2 are the concentrations of bound states 1 and 2, respectively, β is the ratio of the sorbent surface area occupied by state 2 relative to state 1, $k_{a,1}$, $k_{d,1}$, $k_{a,2}$, and $k_{d,2}$ are binding rate constants defined in analogy to the Langmuir model, and k_{12} and k_{21} describe the rates of bound-state changes.

Materials and Methods

Bovine serum albumin (BSA, A 7638, Sigma–Aldrich Corp., St. Louis, MO) and ovalbumin (A 2512, Sigma–Aldrich Corp.) were used for breakthrough experiments at a feed concentration of 1 g/L. The protein was dissolved in 25 mM Tris buffer at pH 8.0 (Sigma–Aldrich Corp.) for the loading step. Loading was followed by a 5–10 column-volume (CV) washing step with 25 mM Tris buffer at pH 8.0. Then, 1 M NaCl in 25 mM Tris buffer pH 8.0 was used to elute the bound protein from the membranes. The capsules were cleaned with 1 M NaCl after each run.

Mustang Q XT5 (axial flow, 5 mL membrane volume) and Mustang Q XT140 (radial flow, 140 mL membrane volume) anion-exchange membrane chromatography capsules were purchased from Pall Inc. (East Hills, NY). Both capsules contain modified hydrophilic polyethersulfone (PES) membranes whose surfaces are coated with an irreversibly cross-linked polymer that contains pendant Q groups. The average effective bed height of the membrane stacks in the XT5 and XT140 capsules is 2.20 mm. The pore size and porosity ε of the membrane are 0.8 μm and 0.70 ± 0.05, respectively (manufacturer data). More details on the internal capsule geometries, including a comprehensive MRI analysis, can be found in a previous publication (Ghosh et al., 2013a). The XT5 capsule was attached to an ÄKTAexplorer system that was controlled by the Unicorn software (GE Healthcare, Uppsala, Sweden). The XT140 capsule was attached to an ÄKTAprocess system that was controlled by the Unicorn software.

Results

In the first paper of this series, lab-scale MC capsules with an axial flow configuration and production-scale MC capsules with a radial flow configuration were comparatively analyzed using 1 mg/mL BSA at a flow rate of 12 CV/min. Non-ideal flow in the lab-scale capsule was effectively captured using a two-zone configuration of the ZRM to describe BTC data obtained under non-binding conditions. The membrane was modeled using the same linear velocity in each zone, as validated by an independent study employing computational fluid dynamics (CFD) (Ghosh et al., 2013b). In contrast, magnetic resonance imaging (MRI) data and CFD simulation both revealed variations in the linear velocity within the membrane stack in the production-scale capsule, and the ZRM was correspondingly configured for describing this capsule (Fig. 3). Several binding models were evaluated. A simplified version of the spreading model, without adsorption/desorption from/to the second bound state, was found to reproduce measured BTCs very well, and provides a coherent explanation of the binding mechanism. Notably, this binding model, combined with different configurations of the ZRM, quantitatively describes BTC data at lab and production scales with the same model parameters. However, model-based scale-up (i.e., prediction of binding BTC data of the production-scale capsule using parameters of the binding model determined at lab scale) was not possible, in part due to the fact that the linear velocity distribution in the production-scale capsule could not be determined from non-binding data.

Here, the linear velocity distribution in the membrane stack of the XT140 capsule is studied as a function of the volumetric flow rate (in membrane volumes per minute, the XT5 and XT140 capsules contain 5 and 140 mL of membrane, respectively). Figure 3b shows that distribution at a flow rate of 12 MV/min. The validity of that distribution is demonstrated through the fact that it was also predicted by CFD simulations in an independent study (Ghosh et al., 2013b). CFD simulations of the same capsule at flow rates of 1.2, 4, and 5.7 MV/min further reveal that the relative distribution of linear flow rates through the membrane is independent of the volumetric flow rate (data not shown). Figure 4 shows

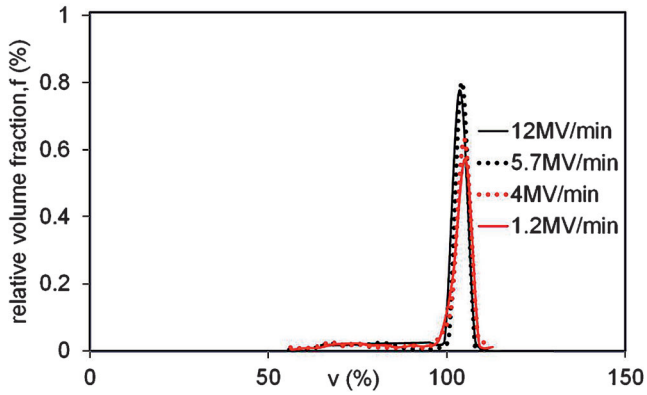

Figure 4. Relative frequency, *f*, of linear velocities, *v*, through the membrane stack at different volumetric flow rates through the production-scale capsule, as determined by fitting a 16-sector ZRM to BTC data measured using BSA (1.2, 4, and 12 MV/min) and ovalbumin (5.7 MV/min) under binding conditions.

that the observed flow-rate-independent velocity distribution, in this case as determined experimentally from BTC data measured under protein binding conditions, can be accurately modeled using a ZRM configured with 16 sectors. The experiments at 1.2 and 4 MV/min were performed with BSA as tracer molecule, while ovalbumin was used at 5.7 MV/min. As predicted by the CFD simulations, the experimentally determined distributions are nearly super imposable, though the width was seen to increase very slightly with decreasing flow rate, likely due to measurement uncertainty. As the effect is indeed quite small, the velocity distribution measured at 12 MV/min was used for all subsequent model calculations, irrespective of the flow rate.

Model-Based Scale-Up for BSA

With the linear velocity distributions known, we asked whether the ZRM could now be used to predict BTC data in the production-scale XT140 capsule. To do this, BTC data for BSA were collected in both the lab and production-scale capsules as a function of feed flow rates.

With the ZRM configured using two membrane zones with the same linear velocity for the lab-scale capsule (Fig. 2), and using one membrane zone and 16 sectors with different linear velocities for the production-scale capsule (Fig. 3), inhomogeneous flow in the hold-up volumes of each capsule was analyzed by regressing the required PFR and CSTR parameters to BTC data measured under non-binding conditions at 1.2 MV/min (Fig. 5a and b) and 4 MV/min (Fig. 6a and b). For both capsules, the configured ZRM reproduces the BTC measured at both flow rates very well. The regressed PFR and CSTR parameters, which are related to the capsule geometry and independent of the binding mechanism, are reported in Tables I and II. Notably, the

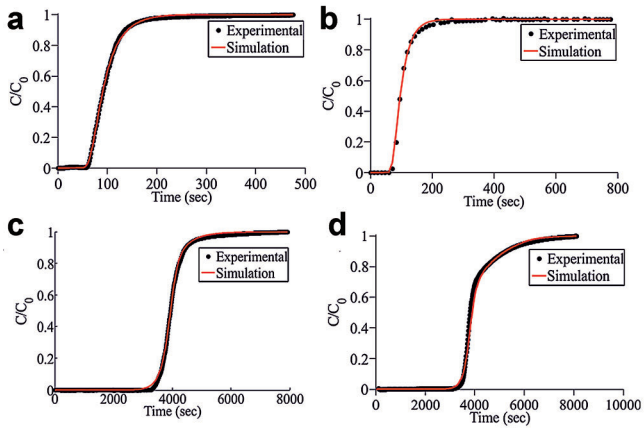

Figure 5. Model-based scale-up for 1 mg/mL BSA at 1.2 MV/min: (**a**) best fit of two-zone ZRM to non-binding BTC of lab-scale capsule, (**b**) best fit of one-zone ZRM with given velocity distribution to non-binding BTC of production-scale capsule, (**c**) best fit to of spreading model combined with two-zone ZRM with fixed PFR and CSTR parameters to binding BTC of lab-scale capsule, and (**d**) predicted and measured binding BTC of production-scale capsule.

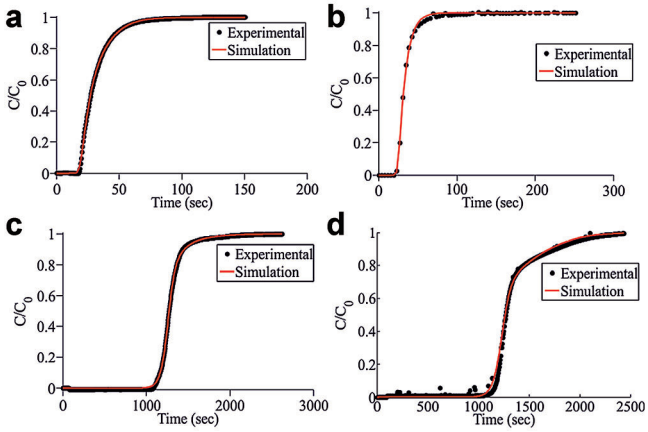

Figure 6. Model-based scale-up for 1 mg/mL BSA at 4 MV/min: (**a**) best fit of two-zone ZRM to non-binding BTC of lab-scale capsule, (**b**) best fit of one-zone ZRM with given velocity distribution to non-binding BTC of production-scale capsule, (**c**) best fit to of spreading model combined with two-zone ZRM with fixed PFR and CSTR parameters to binding BTC of lab-scale capsule, and (**d**) predicted and measured binding BTC of production-scale capsule.

inverse values of the determined residence times approximately follow linear trends over flow rate. This could technically be utilized for predicting these parameters at different flow rates. However, individual determination of these parameters from measurement data at the studied flow rate has been found to yield more accurate results. With these parameters known, the impact of protein binding on BTC behavior in the lab-scale capsule could next be evaluated.

The spreading model was therefore combined with the two-zone ZRM describing flow within the XT5 capsule. Spreading model parameters for BSA binding were then estimated from BTC data measured in that capsule under binding conditions at flow rates of 1.2 MV/min (Fig. 5c) and 4 MV/min (Fig. 6c) and 12 MV/min (Ghosh et al., 2013a). By properly capturing the effects of flow non-idealities in the XT5 capsule, the ZRM configured for that capsule accurately reproduces the BTC at each flow condition. In Table III, the estimated spreading model parameters are reported as a function of flow rate. Each parameter is practically flow rate independent, except for the binding constant $k_{a,1}$. Taking averages of the k_{21} and q_m values observed across flow rates would cause negligible changes in model predictions (data not shown). The initial adsorption rate $1/(k_{a,1} \cdot Q_m) = 0.37$ s (1.2 MV/min), 0.13 s (4 MV/min), and 0.042 s (12 MV/min) is always fast, but increases with flow rate, suggesting either that the protein's surface energy (e.g., conformation) changes with flow, or that the regressed parameter is not intrinsic in nature but contains a small contribution from protein mass-transfer effects.

The goal of this work, however, is not to understand that dependence further, but rather to determine if the ZRM configured for the production-scale capsule with geometry parameters from Table II can be used to predict BTCs in that

Table I. Geometry parameters of symmetric two-zone ZRM of lab-scale capsule operated at different flow rates, as regressed from BTC data measured using 1 mg/mL BSA under non-binding conditions.

Parameter	1.2 MV/min	4 MV/min	12 MV/min
t_{lag} (s)	31.38	7.38	3.91
τ_{inner} (s)	12.02	5.78	1.24
τ_{outer} (s)	22.54	6.60	1.69

preparative-scale unit using parameters for the spreading model (Table III) determined using the scaled-down system. Using that approach, we applied the ZRM configured for the XT140 capsule to predict breakthrough curves for BSA under binding conditions at flow rates of 1.2 MV/min (Fig. 5d) and 4 MV/min (Fig. 6d) within that capsule. Both predictions are in excellent quantitative agreement with experiment. The preparative-scale ZRM not only predicts the point of breakthrough, but also the complex tailing of the BTC as membrane saturation is approached. These predictive results for the full-scale system using binding parameters collected in a scaled-down system are highly relevant for industrial process development, as they prove that binding and breakthrough studies at preparative or pilot scales using potentially scarce and likely expensive pure product are not needed for model development. Instead, any convenient and inexpensive tracer molecule can be applied to define the precise flow non-idealities and thereby configure the ZRM for each scaled unit. Product binding studies conducted in the small-scale unit may then be used to determine all remaining model parameters.

The success of the presented method absolutely depends on the ability of the ZRM to quantitatively decouple band-broadening effects caused by non-ideal flow and non-ideal binding, which are both unavoidable in MC capsules. Binding parameters can only be transferred across scales if this condition is met by the ZRMs configured at the two scales. Finally, the results obtained validate our finding that the linear velocity distribution through membrane in the production-scale capsule is indeed independent of the applied volumetric flow rate.

Model-Based Scale-Up for Ovalbumin

To determine if the scale-up approach described is generally applicable, we next applied it to the same capsules but using a different protein, ovalbumin, at a flow rate of 5.7 MV/min. The ZRM configurations, binding parameter determination and scale-up methodology remained the same as described above. The resulting PFR and CSTR parameters, as shown in Table IV, are in accordance with those obtained with BSA. Moreover, BTCs under non-binding conditions are again reproduced with high accuracy (Fig. 7a and b).

As for BSA, binding of ovalbumin on the PES membrane was quantitatively reproduced and most coherently described by the spreading model (Francis et al., 2011, 2012). Table V shows the binding parameters for ovalbumin determined in the scaled-down unit at a flow rate of 5.7 MV/min. Using those parameters, the ZRM for the XT5 capsule accurately represents ovalbumin breakthrough behavior in that scaled-down system (Fig. 7c).

The ZRM for the production-scale capsule, with the geometric parameters from Table IV, was then combined with the spreading model and binding parameters from Table V to predict the binding BTC of ovalbumin at 5.7 MV/min. As with BSA, the model prediction and measured BTC data are in excellent agreement (Fig. 7d). Both the initial breakthrough point and the approach to saturation of the BTC are quantitatively predicted by the model. The results obtained therefore validate the potential generality of our proposed scale-up method, as well as, our finding that the linear velocity distribution through membrane in the production-scale capsule is not only independent of the applied volumetric flow rate but also of the tracer molecule.

Table II. Geometry parameters of one-zone ZRM of production-scale capsule operated at different flow rates, as regressed from BTC data measured using 1 mg/mL BSA under non-binding conditions.

Parameter	1.2 MV/min	4 MV/min	12 MV/min
t_{lag} (s)	90.50	29.22	9.70
$\tau_{upstream}$ (s)	27.89	9.02	2.99
$\tau_{downstream}$ (s)	4.85	1.56	0.52

Table III. Binding parameters, as estimated by fitting spreading model combined with two-zone ZRM to BTC data of lab-scale capsule measured using 1 mg/mL BSA under binding conditions.

Parameter	1.2 MV/min	4 MV/min	12 MV/min
k_{a1} (1/(g s))	0.90×10^{-2}	2.67×10^{-2}	8.08×10^{-2}
k_{d1} (1/s)	1.06×10^{-5}	1.06×10^{-5}	1.06×10^{-5}
k_{12} (1/(g s))	7.37×10^{-4}	7.37×10^{-4}	7.37×10^{-4}
k_{21} (1/s)	8.02×10^{-3}	9.41×10^{-3}	9.41×10^{-3}
q_m (g/L)	288.8	290.3	289.0
β (−)	1.14	1.14	1.14

The 12 MV/min data are taken from the first paper of this series (Ghosh et al., 2012).

Discussion and Conclusions

The use of scaled-down models of preparative units is a proven strategy for saving material and time in process development. However, few resources are currently available to apply that strategy to MC scale-up. In general, manufacturers of preparative-scale MC units also sell low-volume units that utilize the same membrane chemistry, but

Table IV. Geometry parameters of symmetric two-zone ZRM of lab-scale capsule and of one-zone ZRM of production-scale capsule operated at a flow rate of 5.7 MV/min, as regressed from BTC data measured using 1 mg/mL ovalbumin under non-binding conditions.

Parameter	Lab-scale	Parameter	Production-scale
t_{lag} (s)	4.40	t_{lag} (s)	23.90
τ_{inner} (s)	3.08	$\tau_{upstream}$ (s)	5.80
τ_{outer} (s)	3.31	$\tau_{downstream}$ (s)	0.89

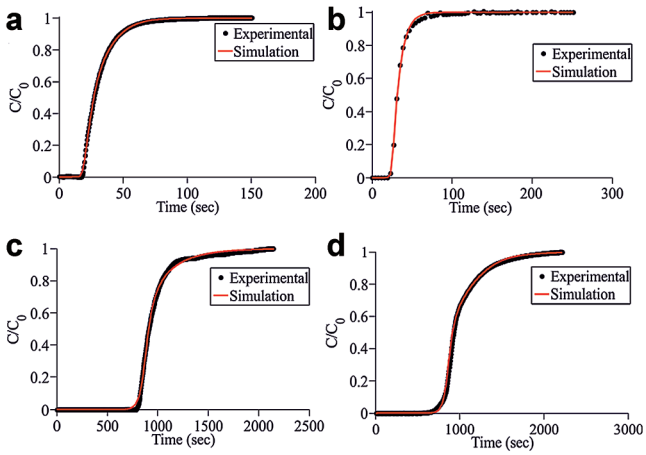

Figure 7. Model-based scale-up for 1 mg/mL ovalbumin at 5.7 MV/min: (**a**) best fit of two-zone ZRM to non-binding BTC of lab-scale capsule, (**b**) best fit of one-zone ZRM with given velocity distribution to non-binding BTC of production-scale capsule, (**c**) best fit to of spreading model combined with two-zone ZRM with fixed PFR and CSTR parameters to binding BTC of lab-scale capsule, and (**d**) predicted and measured binding BTC of production-scale capsule.

not the same membrane arrangement nor the same inlet and outlet flow manifold design. For example, the lab-scale Pall Mustang XT5 capsule utilizes an axial flow design and a 5 mL stack of flat-sheet membranes, while the preparative Pall Mustang XT140 capsule utilizes a radial flow design and a 140 mL membrane stack presented in a pleated-sheet arrangement. Thus, while the low-volume XT5 capsule is well suited for routine laboratory separation needs, it is not designed specifically for process scale-up studies. This fact is demonstrated in Figure 1, which shows that normalized BTCs measured at the two scales differ, notably above ca. 60% saturation.

Here, however, we have shown that results obtained on the geometrically and operationally distinct lab-scale XT5 MC unit can nevertheless be used to accurately predict expected performance in a preparative XT140 unit through application of the ZRM. This is achieved by precisely configuring the ZRM to each unit, thereby permitting contributions to band broadening related to the unique flow non-idealities within each device to be estimated. Those contributions in the scaled-down unit can then be subtracted from overall breakthrough behavior in that unit. The residual defines intrinsic binding non-idealities common to both units, allowing binding parameters obtained from low-cost studies on the scaled-down unit to be directly applied in the ZRM configured for the preparative unit. The present contribution therefore provides proof of concept that the ZRM enables model-based scale-up by conceptually decoupling and independently quantifying the mechanisms of inhomogeneous flow and non-ideal binding in MC capsules at different scales and operating conditions.

Table V. Binding parameters, as estimated by fitting spreading model combined with two-zone ZRM to BTC data of lab-scale capsule measured using 1 mg/mL ovalbumin under binding conditions.

Parameter	5.7 MV/min
k_{a1} (1/(g s))	3.60×10^{-2}
k_{d1} (1/s)	1.40×10^{-5}
k_{12} (1/(g s))	3.20×10^{-3}
k_{21} (1/s)	6.07×10^{-2}
q_m (g/L)	313.6
β	1.55

In a separate publication, we have shown that CFD provides an alternative means to achieve this required decoupling of non-idealities (Ghosh et al., 2013b). However, CFD simulations are computationally expensive and require detailed information on the internal capsule geometry, which can be difficult to acquire. The ZRM is a semi-empirical approach with the same predictive power. It requires estimation of geometry parameters from BTC data for an inexpensive tracer loaded under non-binding conditions. That same information can instead be obtained using CFD models. However, the ZRM approach offers the clear advantage that it is computationally very fast and does not require precise information on internal capsule geometries. Unlike CFD modeling, the ZRM cannot estimate the distribution of linear velocities through the membrane of a given preparative MC unit. However, we show here for the XT140 unit that this distribution is independent of the applied flow rate and tracer molecule used. Consequently, the required distribution can be determined once and for all from only one production scale experiment at binding conditions using a cheap tracer molecule.

The presented work was supported by the Cluster for Industrial Biotechnology (CLIB) with a doctoral scholarship for Pranay Ghosh, as well as by NSERC, the Natural Sciences and Engineering Research Council of Canada.

References

Boi C, Dimartino S, Sarti GC. 2007. Modelling and simulation of affinity membrane adsorption. J Chromatogr A 1162(1):24–33.

Briefs KG, Kula MR. 1992. Fast protein chromatography on analytical and preparative scale using modified microporous membranes. Chem Eng Sci 47(1):141–149.

Brooks CA, Cramer SM. 1992. Steric mass-action ion-exchange—Displacement profiles and induced salt gradients. Aiche J 38(12):1969–1978.

Charcosset C. 2006. Membrane processes in biotechnology: An overview. Biotechnol Adv 24(5):482–492.

Clark AJ, Kotlicki A, Haynes CA, Whitehead AL. 2007. A new model of protein adsorption kinetics derived from simultaneous measurement of mass loading and changes in surface energy. Langmuir 23(10):5591–5600.

Dimartino S, Boi C, Sarti, GC. 2011. A validated model for the simulation of protein purification through affinity membrane chromatography. J Chromatogr A 1218(13):1677–1690.

Francis P, von Lieres E, Haynes C. 2011. Zonal rate model for stacked membrane chromatography. I: Characterizing solute dispersion under flow-through conditions. J Chromatogr A 1218(31):5071–5078.

Francis P, von Lieres E, Haynes C. 2012. Zonal rate model for stacked membrane chromatography part II: Characterizing ion-exchange

membrane chromatography under protein retention conditions. Biotechnol Bioeng 109(3):615–629.

Ghosh R. 2001. Separation of proteins using hydrophobic interaction membrane chromatography. J Chromatogr A 923(1–2):59–64.

Ghosh P, Vahedipour K, Lin M, Vogel JH, Haynes CA, von Lieres E. 2013a. Zonal rate model for axial and radial flow membrane chromatography. Part I: Knowledge transfer across operating conditions and scales. Biotechnol Bioeng 110(4):1129–1141.

Ghosh P, Vahedipour K, Lin M, Vogel JH, Haynes CA, von Lieres E. 2013b. Computational fluid dynamic simulation of axial and radial flow membrane chromatography: Mechanisms of non-ideality and validation of the zonal rate model. J Chromatogr A 1305:114–122.

Ghosh R, Wong T. 2006. Effect of module design on the efficiency of membrane chromatographic separation processes. J Membr Sci 281(1–2):532–540.

Johannes Kiefer, Rasul Nadia H, Ghosh Pranay K, von Lieres Eric. 2014. Surface and bulk porosity mapping of polymer membranes using infrared spectroscopy. J Membr Sci 452:152–156.

Lundstrom I. 1985. Models of protein adsorption on solid-surfaces. Prog Colloid Polym Sci 70:76–82.

Montesinos-Cisneros RM, Lucero-Acuña A, Ortega J, Guzmán R, Tejeda-Mansir A. 2007. Breakthrough performance of large proteins on ion-exchange membrane columns. Biotechnol Appl Biochem 48(Pt 2): 117–125.

Roper DK, Lightfoot EN. 1995. Estimating plate heights in stacked-membrane chromatography by flow reversal. J Chromatogr A 702(1–2): 69–80.

Sarfert FT, Etzel MR. 1997. Mass transfer limitations in protein separations using ion-exchange membranes. J Chromatogr A 764(1): 3–20.

Suen SY, Etzel MR. 1992. A mathematical-analysis of affinity membrane bioseparations. Chem Eng Sci 47(6):1355–1364.

Suen SY, Etzel MR. 1994. Sorption kinetics and breakthrough curves for pepsin and chymosin using pepstatin A affinity membranes. J Chromatogr A 686(2):179–192.

Talbot J, Tarjus G, Van Tassel PR, Viot P. 2000. From car parking to protein adsorption: An overview of sequential adsorption processes. Colloid Surf A-Physicochem Eng Aspects 165(1–3):287–324.

Vogel JH, Nguyen H, Giovannini R, Ignowski J, Garger S, Salgotra A, Tom J. 2012. A new large-scale manufacturing platform for complex biopharmaceuticals. Biotechnol Bioeng 108(12):3049–3058.

von Lieres E, Wang J, Ulbricht M. 2009. Model based quantification of internal flow distributions from breakthrough curves of coin-shaped membrane chromatography modules. Chem Eng Technol 33(6):690–968.

Yang H, Etzel MR. 2003. Evaluation of three kinetic equations in models of protein purification using ion-exchange membranes. Ind Eng Chem Res 42(4):890–896.